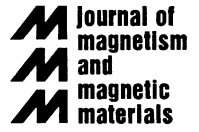




ELSEVIER

Journal of Magnetism and Magnetic Materials 194 (1999) 224–230



# Continuous cell separation using novel magnetic quadrupole flow sorter

Maciej Zborowski<sup>a,\*</sup>, Liping Sun<sup>b</sup>, Lee R. Moore<sup>a</sup>, P. Stephen Williams<sup>a</sup>,  
Jeffrey J. Chalmers<sup>b</sup>

<sup>a</sup>Department of Biomedical Engineering, The Cleveland Clinic Foundation, 9500 Euclid Ave., Cleveland, OH 44195-5254, USA

<sup>b</sup>Department of Chemical Engineering, The Ohio State University, 121 Koffolt Laboratories, 140 West 19th Street, Columbus, OH 43210-1180, USA

---

## Abstract

A laboratory prototype of a flow cell sorter based on magnetic quadrupole field was built and evaluated. The magnetic force acting on magnetically labeled cells in such a field has a 'centrifugal' character which provides a basis for the design of a continuous separation process. The sorter was tested on a model cell system of human peripheral lymphocytes labeled with magnetic colloid. © 1999 Published by Elsevier Science B.V. All rights reserved.

*Keywords:* Quadrupole field; Magnetic colloid; Immunomagnetic separation; Cell separation; Human lymphocytes

---

Rapid cell sorting is important in the newly developing fields of cellular therapy and in biotechnology. Current clinical devices are based on immunoaffinity columns, or on high-gradient magnetic separation (HGMS) columns utilizing either micrometer-sized polymeric beads doped with magnetite, or nanometer-size iron-dextran colloids, conjugated to targeting antibodies [1–3]. We are interested in the development of a fast, continuous process of cell separation based on monoclonal antibodies, magnetic colloid, and a flow field in an open-gradient magnetic field. The continuous separation process offers advantages in the ability to process large cell volumes, use of

on-line monitoring of the separation process, and ability to stage and recirculate sorted fractions. The challenges include exact control over forces involved in displacement of the labeled cell population from the unlabeled population to a degree dictated by the high resolution required between the sorted fractions. The interaction of the magnetic label with the external magnetic field is usually a highly complicated function of spatial coordinates which significantly constrains the number of magnetic field geometries suitable for magnetic flow sorting. A quadrupole magnetic field was selected because of the efficient utilization of the available external magnetic field energy, and because of its highly regular dependence of magnetic force on position. Magnetic quadrupole fields have been tested for continuous dry sorting of coals but were never tested for continuous separation of

---

\*Corresponding author. Fax: +1-216-444-9198; e-mail: zborow@bme.ri.ccf.org.

materials in more viscous media [4,5]. We used a mathematical model of the magnetic and viscous forces to guide us in the design of the flow sorting system. We tested the sorter experimentally using a model cell system of human peripheral lymphocytes targeted with commercial monoclonal antibodies and iron-dextran colloid.

A characteristic feature of an ideal quadrupole field is its linear dependence on the spatial coordinates [6]. In the Cartesian system  $Oxyz$ :

$$\mathbf{B} = [B_x, B_y, B_z] = \frac{B_0}{r_0}[\lambda x, \sigma y, \gamma z], \quad (1)$$

where  $B_x, B_y, B_z$  are components of vector  $\mathbf{B}$ ;  $\lambda, \sigma, \gamma$  are weighting constants, and  $B_0$  is the field magnitude at a characteristic distance  $r_0$  from the origin of Cartesian coordinates (a constant). Divergence of  $\mathbf{B}$  vanishes because there are no point sources of the field  $\mathbf{B}$ :

$$\nabla \cdot \mathbf{B} = 0, \quad (2)$$

where  $\nabla = [\partial/\partial x, \partial/\partial y, \partial/\partial z]$  is the ‘del’ operator, and ‘ $\cdot$ ’ is the symbol of scalar multiplication of two vectors. This imposes the following constraint on the constants  $\lambda, \sigma, \gamma$ :

$$\lambda + \sigma + \gamma = 0. \quad (3)$$

One of the simplest solutions to the above equation is

$$\gamma = 0, \quad \sigma = -\lambda; \quad (4)$$

corresponding to a quadrupole field:

$$\mathbf{B} = \frac{B_0 \lambda}{r_0} [x, -y, 0]. \quad (5)$$

For simplicity we set  $\lambda = 1$  without losing the generality of the argument. Note that the magnitude of vector  $\mathbf{B}$  depends only on the radial coordinate,  $r$ :

$$|\mathbf{B}| = B = \sqrt{B_x^2 + B_y^2} = \frac{B_0}{r_0} \sqrt{x^2 + y^2} = \frac{B_0}{r_0} r. \quad (6)$$

In what follows, we neglect fringing fields at the ends of the pole pieces along  $z$ -axis. The vector plot of the quadrupole field is shown in Fig. 1. The field lines and equipotential lines of the field  $\mathbf{B}$  are shown in Fig. 2. Any set of the equipotential lines can be used to the magnetic pole

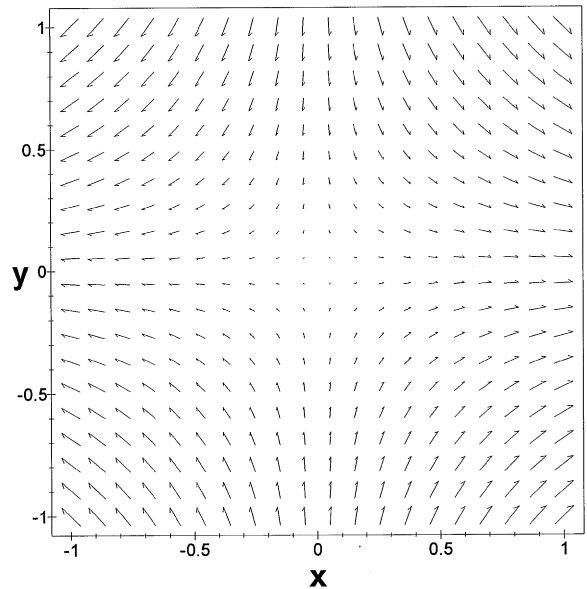


Fig. 1. Vector plot of an ideal quadrupole field  $\mathbf{B}$ . In this and the following two Figures, the units of  $x$  and  $y$  coordinates are arbitrary.

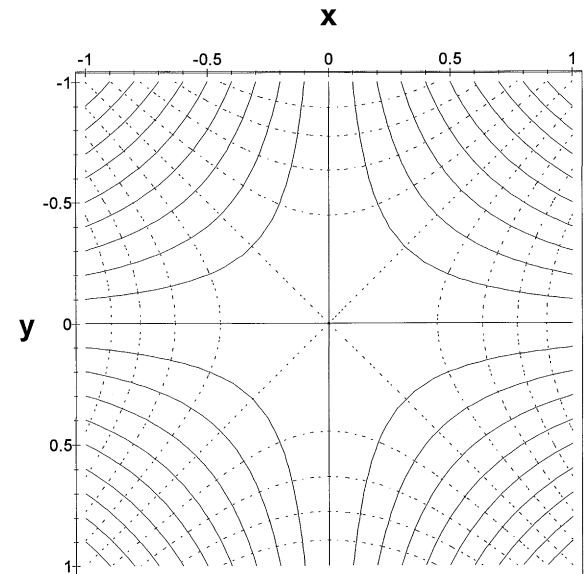


Fig. 2. Equipotential (dashed) and field (solid) line representation of the quadrupole field  $\mathbf{B}$ . Any set of four equipotential lines corresponding to the same magnitude of the field potential may be used to define surfaces of the magnetic pole pieces.

pieces. For the ease of pole piece manufacture, the hyperbolic surfaces are typically approximated by suitable cylindrical surfaces [6].

Magnetic force acting on a point-like magnetic dipole moment  $\mathbf{m}$  is described by the formula [7]:

$$\mathbf{F}_m = (\mathbf{m} \cdot \nabla)\mathbf{B}, \quad (7)$$

where the geometrical interpretation of the expression  $\mathbf{m} \cdot \nabla$  is differentiation with respect to the direction of vector  $\mathbf{m}$  multiplied by the magnitude of vector  $\mathbf{m}$ . Thus, the components of the magnetic force,  $\mathbf{F}_m$ , arise as the result of differentiation along vector  $\mathbf{m}$  of respective components of vector  $\mathbf{B}$ , multiplied by the magnitude of vector  $\mathbf{m}$ . In general, the resulting expression is a complicated function of spatial coordinates which bears no obvious relationship to the vector and field line representations of the magnetic field, Figs. 1 and 2, respectively. The situation improves significantly, however, if one makes a number of simplifying assumptions which apply to a weakly magnetic cell in a magnetostatic field, such as in the case for a magnetically labeled cell in the magnetic separator. The total magnetic dipole moment of a cell is the result of volume magnetization of the magnetic label attached to the cell,  $\mathbf{M}$ :

$$\mathbf{m} = V_m \mathbf{M}, \quad (8)$$

where  $V_m$  is total volume of the magnetic material attached to the cell. The magnetic label is free to rotate in space (together with the cell), and its magnetization is induced by the external magnetic field of strength  $\mathbf{H}$ :

$$\mathbf{M} = \Delta\chi \mathbf{H}, \quad (9)$$

where  $\Delta\chi$  is effective magnetic susceptibility of the label relative to medium. In an isotropic, weakly diamagnetic medium such as water, and for diluted cell suspensions with no free magnetic label in the solution, magnetic fields  $\mathbf{H}$  and  $\mathbf{B}$  differ only by a constant, the magnetic permeability of vacuum  $\mu_0$

$$\mathbf{B} = \mu_0 \mathbf{H}. \quad (10)$$

Combining the last four equations one obtains:

$$\mathbf{F}_m = (\mathbf{m} \cdot \nabla)\mathbf{B} = V_m \Delta\chi (\mathbf{H} \cdot \nabla)\mathbf{B} = \frac{V_m \Delta\chi}{\mu_0} (\mathbf{B} \cdot \nabla)\mathbf{B}. \quad (11)$$

One may take advantage of the following identity, which applies to the special case of time-independent fields (magnetostatic fields) with no electric currents:

$$\nabla(\mathbf{B} \cdot \mathbf{B}) = 2\mathbf{B} \times (\nabla \times \mathbf{B}) + 2(\mathbf{B} \cdot \nabla)\mathbf{B} = 2(\mathbf{B} \cdot \nabla)\mathbf{B}, \quad (12)$$

where the expression containing curl of vector  $\mathbf{B}$  vanishes,  $\nabla \times \mathbf{B} = 0$ , because there are no sources of the field  $\mathbf{B}$  in the cell carrier medium (no time-varying electric fields nor electric currents). Upon substitution to Eq. (11), one obtains a much more intuitive formula:

$$\mathbf{F}_m = V_m \Delta\chi \frac{\mathbf{B}^2}{2\mu_0}, \quad (13)$$

where

$$\frac{\mathbf{B}^2}{2\mu_0} = \frac{|\mathbf{B}|^2}{2\mu_0} = \frac{\mathbf{B} \cdot \mathbf{B}}{2\mu_0} = \frac{1}{2} \mathbf{H} \cdot \mathbf{B} \quad (14)$$

is a measure of magnetic field energy density. Therefore, depending on the sign of  $\Delta\chi$ , magnetic force acting on a magnetized cell follows lines of the steepest ascent ( $\Delta\chi > 0$ ) or the steepest descent ( $\Delta\chi < 0$ ) of the magnetostatic field energy density [8]. The magnetic field energy density distribution in an ideal quadrupole field is axially-symmetric because the magnitude of the field depends only on radial coordinate,  $r$ , Eq. (6). The magnetic force acting on a magnetized cell in the quadrupole field reduces to a particularly simple expression resulting from substitution of Eq. (6) to Eq. (13):

$$\mathbf{F}_m = \frac{V_m \Delta\chi}{\mu_0} \left(\frac{B_0}{r_0}\right)^2 r \left(\frac{\mathbf{r}}{r}\right), \quad (15)$$

where  $B_0$  is the magnetic field at the pole tip located at  $r_0$ . The vector representation of the magnetic force field is shown in Fig. 3. The magnetic force acting on a magnetized particle in an ideal quadrupole field has a ‘centrifugal’ character, that is, it is directed along the radial coordinate of the particle,  $\mathbf{r}$ , and its magnitude increases in direct proportion to the distance from the axis of symmetry,  $r$ . The resulting motion in low viscosity media, such as air, produces outward particle acceleration which increases proportionally to the radial distance [5]. In viscous media, such as water, the radial acceleration of the micrometer-size magnetic particles

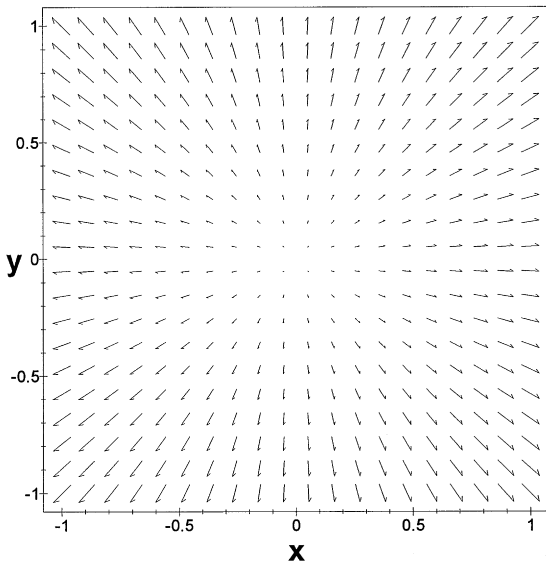


Fig. 3. Vector plot of the force field,  $F_m$ , acting on an induced magnetic dipole in a quadrupole field.

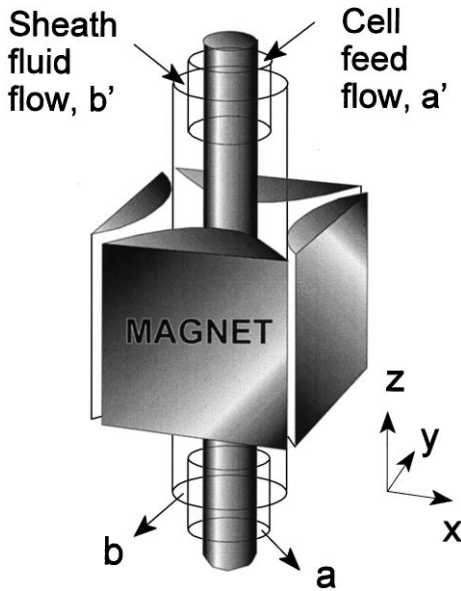


Fig. 4. Schematic representation of the quadrupole flow sorter used in this study. The arrows indicate direction of the fluid flow.

(cells) is small. A highly regular, radial motion of such particles (cells) in the axial flow of the viscous medium provides basis for the continuous cell sorting in the quadrupole field.

A small laboratory prototype was built to test the feasibility of the continuous magnetic cell separation in flowing medium, as shown in Fig. 4. The quadrupole field was generated using permanent magnets (neodymium-iron-boron, maximum energy product of  $2.23 \times 10^5$  T A/m, Dexter Magnetics Corp., Toledo, OH) and suitable pole pieces shaped from soft steel, Fig. 2. The maximum field at the pole tips was  $B_0 = 0.779$  T, the constant field gradient was  $B_0/r_0 = 0.164$  T/mm, the length of the magnet was 76.2 mm, and the magnet aperture was 9.5 mm. The magnetic field was measured using a gaussmeter and Hall-effect probe (Model 9200 Gaussmeter and transverse probe STG920404, F.W. Bell, Orlando, FL, accuracy  $\pm 1\%$  of reading). A precision translation stage (Model 420 X-Y Movement, Newport Corp., Irvine, CA) was used to facilitate precise positioning of the probe in the magnetic field. The field was mapped over approximately 50% of the aperture cross section area, at a spatial resolution of 0.32 mm. A contour plot of the magnetic field magnitude,  $B$ , based on the measured values of its components  $B_x$  and  $B_y$  as a function of  $r = [x, y]$ , shows a high degree of axial symmetry, Fig. 5. Linear regression analysis of  $B$  on  $r$  demonstrates a high degree of linearity, Fig. 6, as expected from Eq. (6).

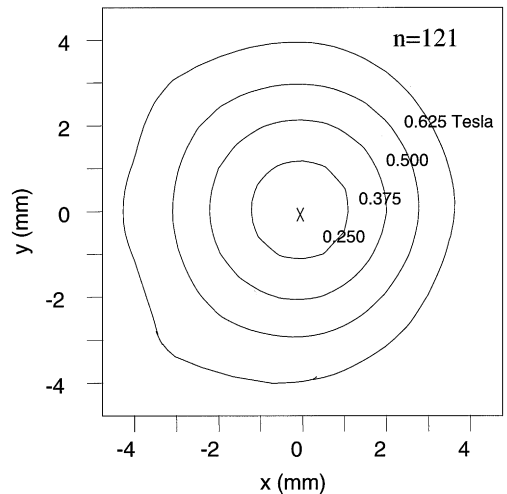


Fig. 5. Contour plot of the magnetic field magnitude,  $B$ , using measured values of field components  $B_x$  and  $B_y$  as a function of  $r = [x, y]$ .

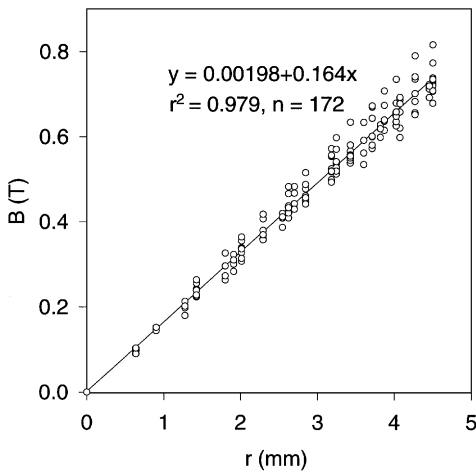


Fig. 6. Measured value of  $B$  as a function of  $r$  (open circles). Solid line represents calculated regression line of  $B$  on  $r$  which was used to extrapolate value of  $B_0 = B(r_0) = B(4.75 \text{ mm}) = 0.779 \text{ T}$ .

The size of the human peripheral lymphocytes used in flow separation experiments, approximately  $7 \mu\text{m}$  in diameter, is such that the effects of Brownian motion may be neglected. The migration path of a cell through the system is therefore characterized by a longitudinal contribution due to its entrainment in the fluid flow along  $z$ -axis, Fig. 7, and a radial contribution due to the interaction of its magnetic labels with the quadrupole field along the radial direction  $r$ , Fig. 3. To a good approximation, longitudinal cell velocity corresponds to the local fluid velocity, which is known for the annular geometry [9], and radial velocity is derived with the use of Eq. (15). An equation describing the resulting cell trajectory has been presented previously [10] in terms of the effective volumetric magnetic susceptibility of the cell, and this may easily be reformulated in terms of cell magnetophoretic mobility. Given the system dimensions, magnetic field strength, volumetric flow rate through the system, and the initial radial position of a cell, this equation allows us to calculate its final radial position for any assumed mobility. We can now apply the concepts of split-flow thin channel (SPLITT) separation technology, developed for thin channels of rectangular cross section (see Ref. [11], for example), to our annular system. This

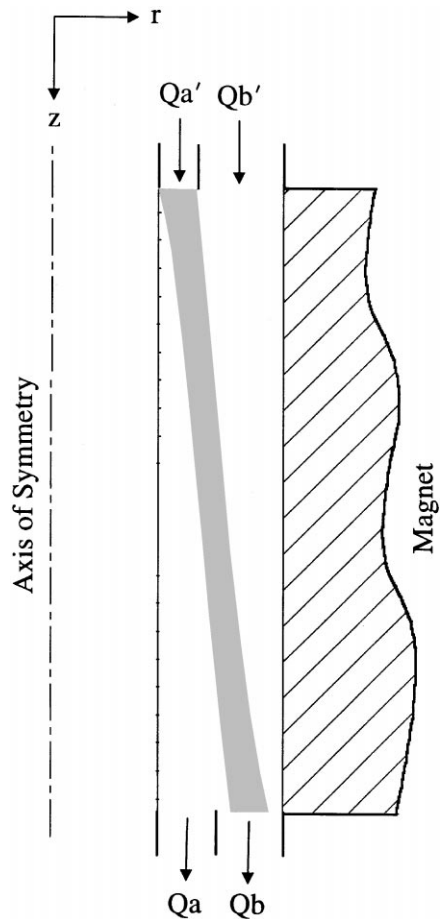


Fig. 7. Concentration distribution of magnetized cells flowing along annular channel inside the quadrupole magnet (flow from top to bottom). The distribution is viewed in the plane containing the axis of symmetry of the magnetic field,  $0rz$ , and shows only half the longitudinal section of the annular channel. The cell suspension enters the field in part of the annular flow indicated by  $Q_{a'}$ , and crosses to the part of the flow provided by the carrier medium,  $Q_{b'}$ . Precise matching of the outlet flows,  $Q_a$  and  $Q_b$ , produces a continuous stream of the magnetized cells in outlet  $b$ , separate from the non-magnetized cells collected in outlet  $a$  (not shown). The gray level of the magnetized cell stream indicates relative cell concentration in the stream (low concentration corresponds to light grey).

approach allows us to determine the required volumetric flow rates at each of the system inlets and outlets to selectively divide a population of cells into two fractions according to some critical level of mobility. Those cells having mobilities greater than this critical mobility are driven into stream lines

that exit the outlet next to the outer wall of the annulus, indicated by flow rate  $Q_b$  in Figs. 4 and 7, while those of a lower mobility remain in streamlines exiting the outlet adjacent to the inner wall, indicated by flow rate  $Q_a$  in Figs. 4 and 7. The required sharpness in cutoff mobility (i.e., the required resolution) effectively fixes the volumetric throughput of the feed stream,  $Q_{a'}$  in Fig. 7, and, given the cell feed concentration, the cell throughput. The flow rate of the cell suspension of the carrier fluid was controlled by syringe pumps (Harvard Apparatus, South Natick, MA) connected to ports  $a'$  and  $b'$  (inlet) and  $b$  (outlet), Fig. 7. Port  $a$  was left open to the atmosphere in order to equilibrate the pressure during the pump operation. The dilution factors for the collected fractions are also fixed by the required flow rate conditions. The combination of experimentally determined cell mobilities [12] with the well characterized quadrupole magnetic separator results in a unique and remarkably powerful preparative technique.

The test cell model consisted of human peripheral lymphocytes collected from apparently healthy volunteer donors who signed a consent form, as approved by the Institutional Review Board. The mononuclear cell (MNC) fraction was isolated by centrifugation on Ficoll cushion. Typical composition of the MNC fraction was 90–95% lymphocytes, with the remainder of the cells identi-

fied as monocytes and a small fraction of erythrocytes. The lymphocytes were targeted using mouse anti-human anti-CD45 monoclonal antibody (mAb) conjugated to fluorescein (FITC) (Becton-Dickinson, Townsend, NJ), and magnetized by a secondary antibody, rat anti-mouse polyclonal antibody conjugated to iron-dextran colloid (MACS microbead, Miltenyi Biotec, Auburn, CA). A small volume of magnetically-labeled lymphocytes was used to spike unlabeled lymphocytes, at a final fractional concentration of 3% labeled cells, to simulate rare cell enrichment by magnetic flow sorting. The binding of the magnetic colloid to target cells increased cell effective magnetic susceptibility,  $\Delta\chi$  in Eq. (15), and made it sensitive to the external magnetic field,  $B$ . The use of the fluorescein stain conjugated to the primary antibody sensitized the target cells to UV light and made them appear as bright cells in the flow cytometry histograms of the cell sample (fluorescence intensity, FI > 100). The unlabeled cells were part of the cell autofluorescence background (FI < 10). In previous studies we have shown that such a labeling procedure produces a one-to-one correspondence between fluorescent and magnetic cell populations [10]. Flow cytometry analyses were performed using a FAC-Scan Analyzer (Becton-Dickinson, San Jose, CA).

The results shown here are part of a larger study [13]. The results presented in this work were

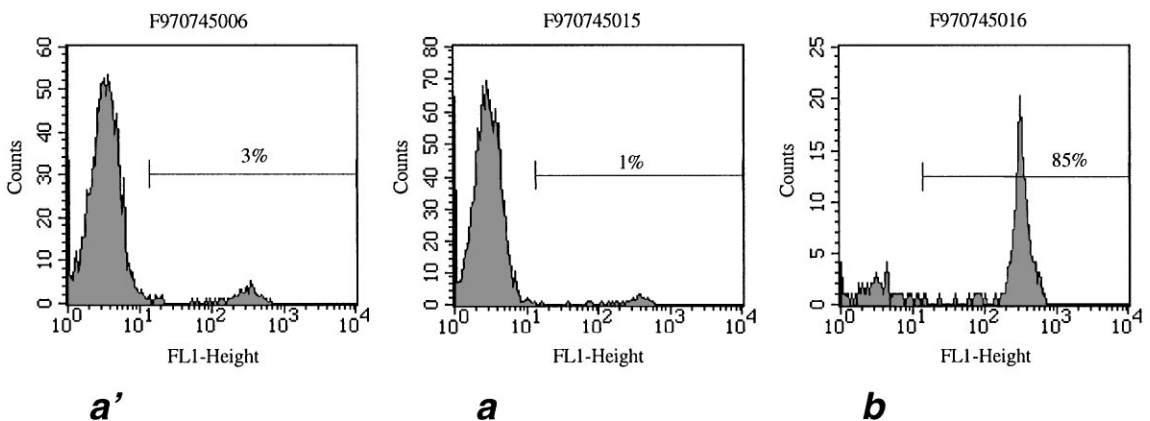


Fig. 8. Cell fluorescence histograms of labeled human CD45 lymphocytes separated from a mixture of unlabeled lymphocytes in the quadrupole flow sorter. Bars and numbers indicate targeted cell fraction (CD45 positive cells).  $a'$  – original sample,  $a$  – non-magnetic cell fraction,  $b$  – magnetic cell fraction. Note significant enrichment of target cells in the magnetic cell fraction ( $b$ ) and depletion of target cells in the non-magnetic cell fraction ( $a$ ).

obtained with the anti-CD45 mAb (three experiments), and they are characteristic of results obtained with other targeting antibodies. Typical total cell concentration in the CD45 cell sorting experiments was  $10^6$  cells/ml, and CD45 cell purity in the feed sample was 3%. Typical total flow rate through the column was 4.0 ml/min, 3% of which was contributed by the flow of the cell sample. The ratio between the outlet flow rates *a* and *b* was 0.25. An example of cell fluorescence histograms in the feed and sorted fractions is shown in Fig. 8. One may note a characteristic increase in the CD45 cell purity in the magnetic fraction *b*, and decrease in the CD45 cell purity in the non-magnetic cell fraction, *a*, as compared to the feed sample. This effect is expected by the inspection of Fig. 7.

The performance of the system was close to the predicted behavior of the magnetic dipole moment in an ideal magnetic quadrupole field. The flow of the viscous fluid medium (aqueous cell carrier) contributed a resistive element to the magnetic separation process. By changing the resistance to cell transport along the magnetic field gradient, we were able to control the composition of the sorted cell fractions (purity and recovery, not shown). Such control is unique for the continuous sorting process, and cannot be achieved with the existing batch magnetic cell separators. The combination of small, colloidal magnetic labels, and the continuous magnetic sorting process may lead to the development of a magnetic flow sorting method based on cell surface antigen expression [14].

### Acknowledgements

This work was supported by grants NIH R01 CA62349 (M.Z.) and Whitaker Foundation (J.J.C.).

We would like to thank Mr. Jim Proudfit for expert technical help in machining parts of the magnetic flow sorter.

### References

- [1] K. Auditore-Hargreaves, S. Heimfeld, R.J. Berenson, *Bioconjugate Chem.* 5 (1994) 287.
- [2] J. Ugelstad, P. Stenstad, L. Kilaas et al., *Blood Purif.* 11 (1993) 347.
- [3] A. Radbruch, B. Mechtold, A. Thiel et al., *Meth. Cell Biol.* 42 (1994) 387.
- [4] P.A. Liberti, B.P. Feeley, in: D.S. Compala, P. Todd (Eds.), *Cell Separation Science and Technology*, ACS Symp. Series 464, ACS, Washington, DC, 1991.
- [5] R.D. Doctor, C.B. Panchal, C.E. Swietlik, *Recent Advances in Separation Techniques-III*, AIChE Symp. Series, 82, 1986, p. 154.
- [6] P.H. Dawson, in: P.H. Dawson (Ed.), *Quadrupole Mass Spectroscopy and Its Applications*, Elsevier, New York, 1976.
- [7] R. Becker, *Electromagnetic Fields and Interactions*, Dover, New York, 1982.
- [8] M. Zborowski, in: U. Hafeli, W. Schuett, J. Teller, M. Zborowski (Eds.), *Scientific and Clinical Applications of Magnetic Microcarriers*, Plenum Press, New York, 1997.
- [9] R.B. Bird, W.E. Stewart, E.N. Lightfoot, *Transport Phenomena*, Wiley, New York, 1960.
- [10] M. Zborowski, S. Williams, L. Sun et al., *J. Liq. Chrom. Rel. Tech* 20 (1997) 2887.
- [11] J.C. Giddings, *Sep. Sci. Technol.* 27 (1992) 1489.
- [12] S. Reddy, L. Moore, M. Zborowski et al., *Chem. Eng. Sci.* 51 (1996) 947.
- [13] L. Sun, Ph.D. Dissertation, The Ohio State University, Columbus, OH, 1998.
- [14] J.J. Chalmers, M. Zborowski, L. Sun et al., *Biotechnol. Progr.* 14 (1998) 141.